NASA-TM-111794

IN-24-TM

IMPACT CHARACTERISTICS OF CANDIDATE MATERIALS FOR SINGLE-STAGE-TO-ORBIT (SSTO) TECHNOLOGY

Alan Nettles
NASA/Marshall Space Flight Center
Mail Code EH33
Huntsville, AL 35812

ABSTRACT

Four fiber/resin systems were compared for resistance to damage and damage tolerance. One toughened epoxy and three toughened bismaleimide (BMI) resins were used, all with IM7 carbon fiber reinforcement. A statistical design of experiments technique was used to evaluate the effects of impact energy, specimen thickness and tup diameter on the damage area and residual compression-after-impact (CAI) strength. Results showed that two of the BMI systems sustained relatively large damage areas yet had an excellent retention of CAI strength.

KEY WORDS: Impact Resistance, Delamination Resistance, Non-Destructive Evaluation

1. INTRODUCTION

As NASA sets its sights on single stage to orbit (SSTO) reusable vehicles, the need for weight reduction is becoming critical. These vehicles must use advanced materials that possess a multitude of improved properties (lower density, higher stiffness and strength, resistance to damage and moisture absorption, good fatigue resistance, high temperature stability and resistance to microcracking due to thermal cycling) compared to conventional aerospace materials. Aerospace vehicles are beginning to contain more polymer matrix composites as load bearing structures in order to lower weight.

In order for a thermoset polymer to withstand high temperatures without a degradation of mechanical properties, a high cross-linking density is desired. However, a high cross-linking density will result in a brittle material which will not provide a damage tolerant matrix for the composite. Some thermoplastic resins such as Polyetheretherketone (PEEK), polybenzimidazole (PBI) and polyallylphenols can withstand higher temperatures than thermoset resins, and have the additional bonus of being inherently tough. However, thermoplastic matrix composites, which are difficult to handle since they have no tack or drape, require high temperatures and pressures to process. By blending thermoplastics into thermosets, the resulting polymer can be engineered to have a good balance of high temperature resistance, damage tolerance, and processability.

A class of polyimides called bismaleimides (BMI's) have the processability of epoxies with the higher use temperatures common to polyimides. BMI's are polyimides that contain a

vinyl group as part of the five membered imide ring, resulting in an uncured prepreg that has good tack and drapeability and will process at 350°F and 80 psi (or lower) much like epoxies. Unlike epoxies, the BMI composite must undergo a free-standing post-cure, usually at a temperature of about 475°F for 8 hours. BMI resins cannot match the temperature capabilities of PMR-15, since the upper use temperature of most BMI's is about 450°F under dry conditions and 390°F under wet conditions, but this is a substantial increase (about 200°F) over epoxies. Like all polyimides, BMI is inherently brittle and must be modified with a "toughener" to be of any use as a matrix resin for advanced aerospace structures. Thus about 25 to 50% by weight thermoplastic is blended with the BMI to improve its damage tolerance (1). Some blends have demonstrated a resistance to microcracking when thermally cycled from -108°F to 350°F making them as microcrack resistant as cyanate resin systems (2). Different thermoplastics in a variety of amounts are used to engineer the matrix resin to have the most desirable properties for the application at hand. In general, BMI resins with the highest room temperature mechanical properties would be the most affected by heat, losing a larger percentage of strength with increasing temperature than those resins designed for hot environments which tend to have lower room temperature mechanical properties (3).

This paper examines the impact resistance and damage tolerance of four aerospace grade polymer matrix systems that have been identified as candidate materials for some of NASA's Single Stage to Orbit (SSTO) programs. One of these systems is a toughened epoxy and the other three are toughened BMI resins. All of these materials contained the same fiber (Hercules' IM7) so a comparison of the matrix resins could be made without the type of reinforcement being an additional variable.

2. EXPERIMENTAL DESCRIPTION

2.1. Material The four fiber/resin systems used in this impact damage tolerance study were IM7/977-2 epoxy, IM7/V390, IM7/V398 and IM7/F655 BMI's.

The 977-2 epoxy produced by ICI/Fiberite is the best characterized and most widely used toughened epoxy system. The V390 and V398 BMI's are produced by Hitco and differ in their toughness and upper use temperature. The V390 resin possesses a hot/wet performance temperature of 475°F while the tougher V398 resin has a hot/wet use temperature of 350°F. The F655 BMI resin is produced by Hexcel and has an upper use temperature of 450°F. This resin was designed primarily to have easy processing characteristics and enhanced damage tolerance.

2.1.1 Specimen Preparation Panels were made of unidirectional prepreg layed up in a quasi-isotropic stacking sequence of $[0,+45,90,-45]_{ns}$, where n was either 1,2 or 3 thus producing 8, 16 or 24 ply laminates. The panels were hot-press cured according to the manufacturer's recommendations. Specimens 17.8 cm (7 inches) long by 7.6 cm (3 inches) wide were cut from the cured panels and fiberglass end tabs 3.8 cm (1.5 inches) long were bonded to the ends of each specimen. The cured nominal ply thicknesses for the various materials were .1219 mm (.0048 in.), .1372 mm (.0054 in.), .1168 mm (.0046 in.) and .1168 mm (.0046 in.) for the 977-2, F655, V390 and V398 respectively.

2.2. Testing

2.2.1. Test Matrix A design of experiments approach was used to construct a test matrix that would evaluate the effects of impact level, plate thickness and impactor diameter on the compression-after-impact (CAI) strength and damage area of the plates. A Box-Behnken 3 level fractional factorial design was implemented to minimize the number of tests needed to gather information about the effects of the 3 independent variables on the damage zone size and CAI strength. Utilizing this method, a total of 15 tests would need to be run on each material type. Each independent variable (impact level, plate thickness and impactor diameter) was assigned 3 values representing a low, medium and high setting. For the impact level, a low value was defined to be an incident kinetic energy of 4 joules (2.95 ft-lbs), a medium level was 8 joules (5.90 ft-lbs) and a high level was 12 joules (8.85 ft-lbs). The thickness of the specimen was determined by the 3 thicknesses

fabricated, low = 8 plies, medium = 16 plies and high = 24 plies. Tups of diameter .635, 1.27 and 1.9 cm (.25, .5 and .75 in.) were used as the low, medium and high values of impactor size. The test matrix with the variables at the appropriate levels is shown in figure 1.

2.2.2 Impact Testing The specimens were pneumatically clamped between plates with cutout holes of 6.35 cm (2.5 in.) diameter thus inducing a circular clamped boundary condition. Each specimen was impacted at its geometric center. A Dynatup 8200 drop tower was used with a falling mass of 2.3 kg (5.0 lbs). A catch mechanism was employed to prevent multiple strikes on the specimens. Instrumented impact data (such as incident impact velocity, maximum load of impact, total deflection and energy absorbed during impact, as well as load-time and load-deflection plots for the impact event) were gathered with a Dynatup 730 data acquisition system. After each impact, the visual damage was noted and recorded.

2.2.3. NDE Evaluation After impact testing, all of the specimens were ultrasonically C-scanned to obtain a damage zone size.

2.2.4. Compression Testing Residual compressive strengths of the impacted specimens were obtained using a face supporting, shear loading technique explained in detail elsewhere (4). Basically, this fixture is a large IITRI type with faceplates clamped lightly to most of the specimen's gage length to prevent Euler buckling. The faceplates contained cutouts at their centers to allow the delaminations to "blister out" and grow. An Instron 1100 loading frame was used at a testing rate of .254 mm/min. (.01 in./min.).

2.2.5. Short Beam Shear Testing Short beam shear specimens were prepared from randomly selected, unimpacted 24 ply specimens. The specimens were .635 cm (.25 in.) wide tested at a span of 1.27 cm (.50 in.). Testing was performed at a rate of .254 mm/min. (.01 in./min.).

2.2.6. Double Cantilever Beam Testing Double cantilever beam (DCB) specimens were prepared from IM7/977-2 carbon/epoxy and IM7/V390 Carbon/BMI material systems. Specimens were of a $[0,+45,90,-45]_{2S}$ lay-up with a total length of 25.4 cm. (10 in.) and width of 2.54 cm. (1 in.). A Teflon film insert was placed between the centermost 90/-45 interface at a distance of approximately 5 cm. (2 in.) from an end in order to obtain a starter crack. Testing was performed at a crosshead rate of 50 mm/min. (2in./min.) and the value of G_{IC} was determined by the load/displacement area method.

3. EXPERIMENTAL RESULTS

3.1. NDE Testing All of the impacted specimens showed delaminations as indicated by the ultrasonic scanning results. All of the samples that were 16 or 24 plies thick showed circular areas of delamination. The 8 ply specimens showed delamination areas that were longer in the 0° (outer fiber) direction. This is due to the lower bending stiffness of the thinner laminates producing a much higher outer fiber membrane strain which tended to break these fibers and split the matrix along the direction of these fibers. The C-scans, along with maximum impact load and residual compression strength data are presented in figures 2a-d. A relatively large damage area is seen on the V390 and V398 specimens compared to the F655 and 977-2 resins for almost all of the runs. The only exceptions are the specimens that were completely penetrated by the impactor. In these cases, the apparently "tougher" 977-2 and F655 resins would resist splitting and cracking more, resulting in the broken fibers "carrying" more of the resin away from the laminate resulting in delamination. The apparently less tough V390 and V398 resins would produce a "cleaner" hole when punctured since the resin would more easily crack and split, allowing the broken fibers to separate from the laminate with less far field matrix damage. For the V398 and V390 samples that did not experience perforation, the damage zone extended to the boundaries of the circular clamp. This makes a true assessment of "damage resistance" difficult since the damage area would have been much greater had the delaminations not stopped at the clamped boundary. The 977-2 and F655 materials had delaminations that were contained well within the clamped boundary.

3.2. Short Beam Shear Testing A large difference in mode II interlaminar shear strength was evident between the materials tested. The delamination always initiated at one of the two centermost 90°/-45° interfaces. The results of the short beam shear tests are given in figure 3. The V390 and V398 resin composites had much lower interlaminar shear strength than the F655 or 977-2 resin composites which explains the larger delamination areas seen in the V390 and V398 resin laminates after impact.

3.3. CAI Testing All of the specimens failed at the impact site. The V390 and V398 resin system laminates do not have a noticeably lower CAI strength than the 977-2 and F655 resin system laminates as would be expected from the NDE results. The drop in strength is not as large as would be indicated by the C-scans. The C-scans clearly show that the V390 and V398 resin laminates have a larger delamination area than the 977-2 and F655 resin laminates, but the V390 and V398 resin laminates do possess good damage tolerance since these large areas of damage do not cause a correspondingly large drop in compression strength. This phenomenon will be examined in detail later.

3.4. Double Cantilever Beam (DCB) Testing (G_{IC} Testing) The V390 material was found to have a G_{IC} of approximately .92 kJ/m^2 (5.2 in-lb/in^2) and the 977-2 had a G_{IC} value of approximately 1.25 kJ/m^2 (7.3 in-lb/in^2). This difference is not as large as the difference in mode II shear strength as determined from the short beam shear tests.

3.5. IM7/977-2 Material The model terms for the CAI strength and damage area responses are given in figure 4. There is a strong non-linearity between the CAI response and the impact energy as well as a strong negative linear effect. This can be seen on the response surface plot of CAI strength as a function of impact energy and specimen thickness shown in figure 5. There is a sharp drop in strength as the impact energy increases from the lowest level, but the strength decrease begins to level off near the higher end of impact energy with a slight increase in CAI strength seen at the highest impact energies. This is due to the specimen beginning to be punctured at these higher impact levels, resulting in more fiber damage and less matrix damage which is the controlling factor for residual compression strength of the laminate. There are not any significant two-way interactions for the CAI response and the value of the tup setting is not significant for either of the responses. The damage zone is most heavily dependent on the linear impact energy coefficient which indicates that as the impact energy increases, the area of damage also increases. This response also shows an interaction between impact energy and specimen thickness. As can be seen from figure 6, at the lower end of impact energies used in this study, the smallest damage areas occurred on the intermediate thickness specimens. The thick specimens had more flexural rigidity and thus could not absorb as much of the impact energy as bending strain energy thereby causing this energy to be dissipated by matrix damage. The thinnest specimens could flex quite a bit and the fibers would store plenty of elastic strain energy, but the deformations were large enough to cause matrix splitting between fibers, especially in the outer fiber direction as is evident by the C-scans in figure 2a. At the higher values of impact energy used in this study, the thinner the specimen, the more damage area resulted. This is due to the fact that the tup would puncture the thinner specimens resulting in gross fiber pullout along the outer fiber direction as is evident by the C-scans in figure 2a. This larger area of damage contributed to a loss in CAI strength on the thin samples, as seen in figure 5, since the damage was completely through the thickness.

3.6. IM7/F655 Material From figure 7 which is a response plot of CAI strength versus impact energy and specimen thickness, it can be seen that this material has a non-linear dependence on the impact energy. It has a similar shape to the IM7/977-2 composite CAI response in that the sharp drop in residual compression strength begins to level off at the higher end of impact energies used. The model terms are given in figure 8. The linear coefficient of impact energy is the strongest term at -53 MPa while the quadratic coefficient for this independent variable is 37 MPa. The linear thickness coefficient is quite large at 45 MPa with a quadratic coefficient of -15 MPa. This indicates that the thinner specimens had less strength than the thicker specimens, with this trend decreasing a small amount as the thickness increases (a leveling off). The tup size had a small effect on the CAI strength and damage area responses. A larger tup produced a larger CAI strength than the thinner tups, but this was dependent on the impact energy used as is evident by the interaction term for

both responses. In fact, the impact energy/tup size interaction term for the damage area response is greater than the linear or quadratic coefficients for the tup size on this response. Figure 9 shows the CAI strength response surface as a function of impact energy and tup size. At the high end of impact energy, the tup size had little effect on the CAI strength response and showed only a slight increase in strength with increasing tup size. However, at the lower impact energy levels, the tup size became more important and showed a larger increase in strength with increasing tup size. Figure 10 shows the damage area response surface as a function of impact energy and tup size. This plot indicates that at low values of impact energy, the smallest tup size gave the largest damage area which corresponds with the CAI strength observations. However, at high impact energies the damage area was much greater for the larger tup. This larger damage area did not correspond to a drop in CAI strength, mainly due to the results obtained on runs # 1 and #2 which had the tup size at the two extremes and the largest impact energy used. Run #1 had a larger area of damage as detected by ultrasonics, but has a slightly higher CAI strength than the specimen in run #2. Since tup size does have an effect on the CAI strength, this material may have a compression failure mechanism that is not as heavily dependent on absolute 2-D matrix damage size as epoxies, but is also dependent on the amount of through-the-thickness matrix damage and/or fiber breakage since the smaller tup tended to break more fibers and cause more through-the-thickness matrix damage.

3.7. IM7/V398 Material The model terms for this material (figure 11) are quite different from the 977-2 and F655 resin systems, most notably the strong dependence of damage area on specimen thickness and the relatively smaller effect of impact energy on CAI strength. Figure 12 is a surface response plot of CAI strength as a function of impact energy and specimen thickness. This material is surprisingly insensitive to impact energy, especially on the thicker specimens. On the thinner specimens a decrease in CAI strength is seen with an increase in impact energy. However, note that the quadratic impact energy coefficient is *negative* which implies that a sharp drop in CAI strength is seen only at larger impact energies as the impact energy increases. This is the opposite trend from the 977-2 and F655 resin systems where as the impact energy increased at larger values of impact energy, a puncture type of damage was formed and the drop in compressive strength began to level off. The trend in the V398 material suggests that the CAI strength may be more dependent on through-the-thickness damage and/or fiber breakage than absolute 2-D matrix damage size (a characteristic that was noticed to a small extent in the F655 material). The effects of specimen thickness on the CAI strength is very non-linear with the strength showing a rapid decrease as the specimen gets thinner which again suggests that through-the-thickness damage and/or fiber breakage (which was more pronounced on the thinner specimens) has a strong influence on the CAI strength of the specimens.

The tup size also had an effect on the CAI strength of the specimens as is evident by the plot in figure 13 which shows CAI strength as a function of impact energy and tup size. At the low levels of impact energy, the tup size had little effect on the residual compressive strength but at the higher impact energies, a smaller tup would be more detrimental to the residual compression strength (a strong interaction coefficient shows this). Since the smaller tups tended to cause a puncture at the higher impact energies than the larger tups, this again suggests that the CAI strength of this material is dependent upon the amount of through-the-thickness damage and/or fiber breakage and not on the absolute 2-D size of matrix damage as detected by C-scans.

The damage area caused by the impact was most influenced by the thickness of the specimen and little else as is evident from the coefficients in figure 11. The tup size had no effect on the damage area and the impact energy had a small effect but this response is clearly dominated by the specimen thickness which can be graphically seen in figure 14. The damage area is linearly dependent on the specimen thickness with the thicker specimens showing much more damage area than the thinner specimens, regardless of impact energy (no interaction between these variables). As can be seen in the C-scans in figure 2c, the thin specimens had a more elongated damage area indicating matrix splitting which is a through-the-thickness type of damage. The damage area varies non-linearly with impact energy with the lower impact energies giving less damage area This trend leveled off around the medium values of impact energy after which the impact energy had little effect on the measured damage area, since as mentioned earlier, the damage zone did not spread beyond the circular clamped boundaries of the plate.

3.8. IM7/V390 Material The CAI strength of this material varies linearly with specimen thickness, the thicker specimens having a higher CAI strength. This dependence is quite significant as is evidenced by the linear thickness coefficient seen in figure 15 and the plot of CAI strength versus impact energy and specimen thickness shown in figure 16. The impact energy has a non-linear effect on the CAI strength with the same trend seen as for the V398 material, and has a more pronounced effect on the residual compression strength at the higher impact energies. The "leveling off" of strength decrease is not at the higher end of impact energies as it is for most epoxies and the F655 BMI tested in this study. Another unique feature of this material is the effect of the tup size on the CAI strength of this material. The tup alone has no effects on the CAI strength as can be seen by the zero coefficients for linear and quadratic tup terms in figure 15. However, there are strong tup interaction terms with the other two variables. The interaction between tup size and impact energy can be seen in figure 17 which is a plot of CAI strength as a function of impact energy and tup size. At the small tup size, the impact energy shows a non-linear drop in compression strength as the impact energy increases. When the tup is at the larger sizes, the CAI strength actually increases (albeit a very small amount) with increasing impact energy before a drop in strength is seen at the medium levels of impact. At the low levels of impact, increasing the tup size tended to decrease the CAI strength, a trend not seen in any of the other materials, but at the high impact levels, the larger tup showed little degradation of the CAI strength, especially when compared to the smaller tup sizes.

The tup size also had a strong interaction with the specimen thickness on the CAI response of the material as can be seen in figure 18. At small tup sizes the CAI strength did not depend heavily on the specimen thickness but at large tup sizes the CAI strength was much greater for thicker specimens. This once again indicated that specimens that have sustained fiber damage (those that have been punctured) such as thin specimens hit with a large tup or thicker specimens hit with a small tup, have a larger decrease in residual compression strength than those specimens that have sustained an impact where a heavy matrix damage area (not volume) has occurred, but little or no fiber breakage has occurred. The thin specimens saw a decrease in CAI strength as the tup was made larger but the thicker specimens saw a decrease in CAI strength as the tup size became smaller. This can be explained by the thinner specimens sustaining a puncture type of damage regardless of tup size, thus a larger tup will produce a bigger hole resulting in more damage. For the thicker specimens only the small tup could puncture the specimens and cause the fiber damage that seems to be associated with the decrease in the residual compressive strength.

The tup size had no effect on the damage size that was created due to the impact event except for a very small interaction with impact energy. The damage area was strongly dependent on the specimen thickness in a non-linear manner as is shown in figure 22 which is a plot of the response surface of damage size as a function of impact energy and specimen thickness. A sharp drop in damage area is seen as the specimen becomes thinner. This is due to a hole being punctured in the specimen and the damage being more localized in the form of fiber breakage and matrix splitting. For this reason the impact energy did not have as big an effect on damage size for the thin specimens as it did for the thicker specimens.

3.9. CAI Strength Vs Damage Area Figures 20,21 and 22 show plots of CAI strength vs. delamination area for the 8, 16 and 24 ply specimens. For the 8 ply specimens, there is little correlation between damage area and CAI strength. For the 16 and 24 ply specimens, the 977-2 and F655 systems show a much lower CAI strength as the damage area increases, for the V390 and V398 resins however, the CAI strength is relatively independent of damage size.

4. CONCLUSIONS

4.1. Summary of Experimental Results From the experimental data, the following can be concluded:

- The V398 and V390 laminates behave similarly and the F655 and 977-2 laminates behave similarly in both CAI and damage area developed. The two sets behave quite differently.

• The V398 and V390 resin systems have a much lower mode II delamination resistance and thus produce larger damage zones as detected by ultrasonic scanning. This does not apply to the 8 ply specimens since they experience a puncture type of damage (fiber breakage and/or longitudinal matrix splitting).
• The V398 and V390 materials do not have as large of a drop in compression-after-impact strength as the 977-2 and F655 materials.
• The 977-2 and F655 laminates have "classical" CAI vs. Impact Level plots (i.e. the strength drops off sharply at the early stages of damage and then levels off with increasing impact energy). The V398 and V390 laminates show no sharp drop in CAI strength until high levels of impact are reached.
• The V398 (and to a lesser extent the V390) 16 and 24 ply laminates show very little change in CAI strength regardless of damage size.

5.REFERENCES

1. Stenzenberger,H.D., Herzog,M., Konig,P. Rome,W and Breitigan,W., "Bismaleimide Resins: Past, Present, Future," *Proc. 34th Int. SAMPE Sym.*, 1989, pp.1877-1888.

2. Konarski,M.M., "V-391: A Novel Composite Matrix With the Temperature Performance of BMI's and the Toughness of Thermoplastics," *Proceedings of the 34th Int. SAMPE Sym.*, 1989, pp. 505-513.

3. Stenzenberger,H.D. ,Konis,P. ,Romer,W. , Herzog,M and Breitigan,W.V., "BMI/(Bis(Allylphenoxyphthalimide)) - copolymers: A new family of Resins for Advanced Composites with Improved Thermal Oxidative Stability," *Proceedings of the 36th Int. SAMPE Sym.*, 1991, pp. 1232-1241.

4. Nettles,A.T. and Hodge,A.J., "Compression-After-Impact Testing of Thin Composite Materials," *Proceedings of the 23rd Int. SAMPE Sym.*, 1991, pp. 177-183.

Run #	Impact Energy	Thickness	Tup Size
1	+1	0	+1
2	+1	0	-1
3	-1	0	+1
4	-1	0	-1
5	+1	+1	0
6	+1	-1	0
7	-1	+1	0
8	-1	-1	0
9	0	+1	+1
10	0	-1	+1
11	0	+1	-1
12	0	-1	-1
13	0	0	0
14	0	0	0
15	0	0	0
	-1 = 4J	-1 = 8 plies	-1 = .25 in.
	0 = 8J	0 = 16 plies	0 = .5 in.
	+1 = 12J	+1 = 24 plies	+1 = .75 in.

Figure 1. Run Summary for impact tests.

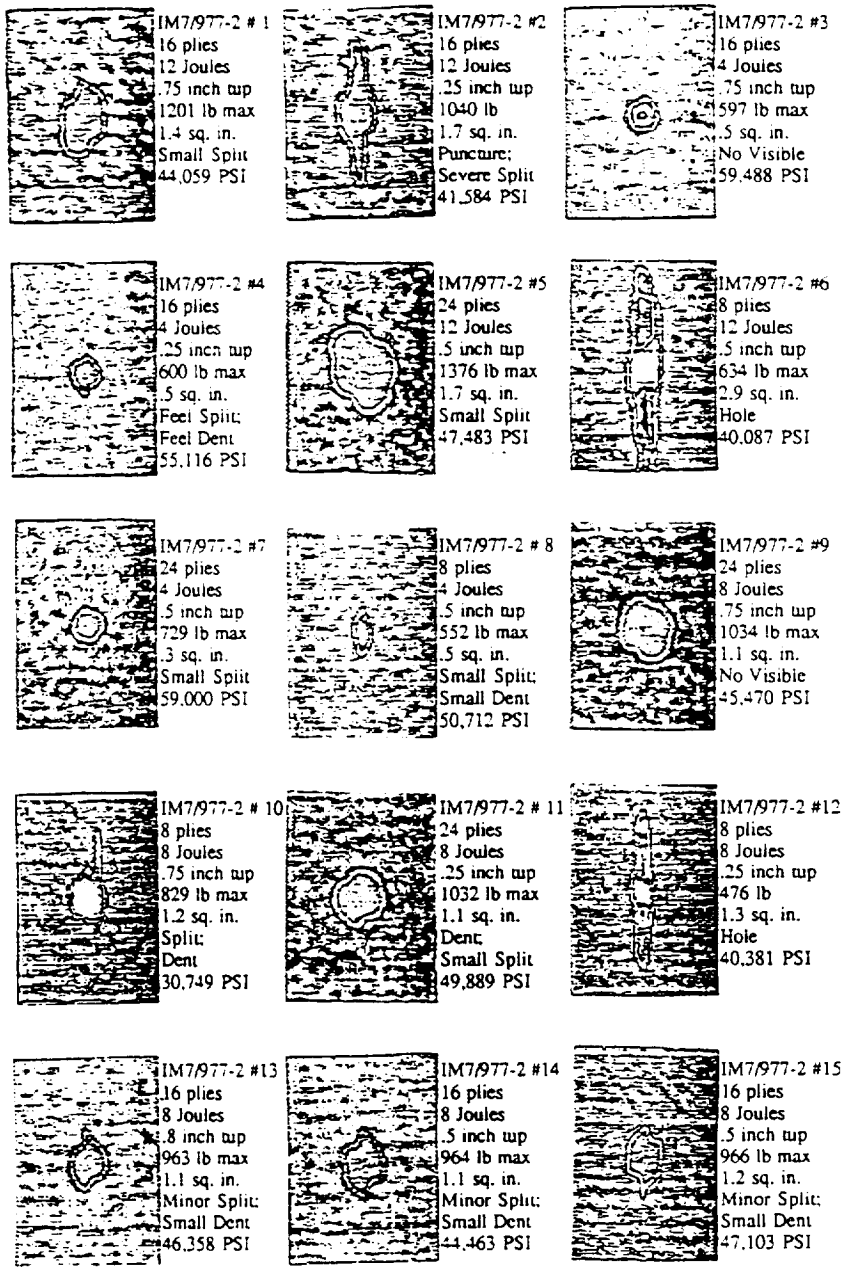

Figure 2a. C-Scans and associated maximum load of impact, damage area, visual damage and residual strength data (IM7/977-2).

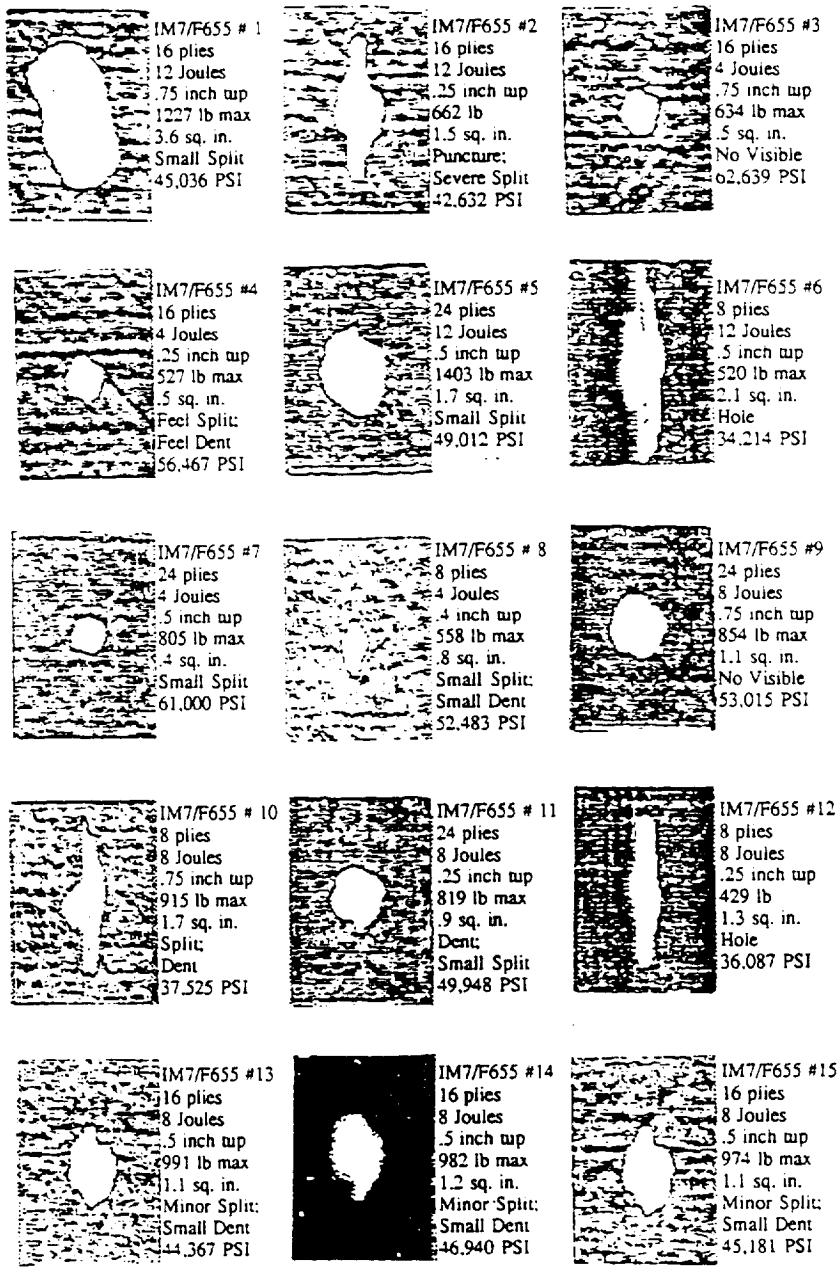

Figure 2b. C-Scans and associated maximum load of impact, damage area, visual damage and residual strength data (IM7/F655).

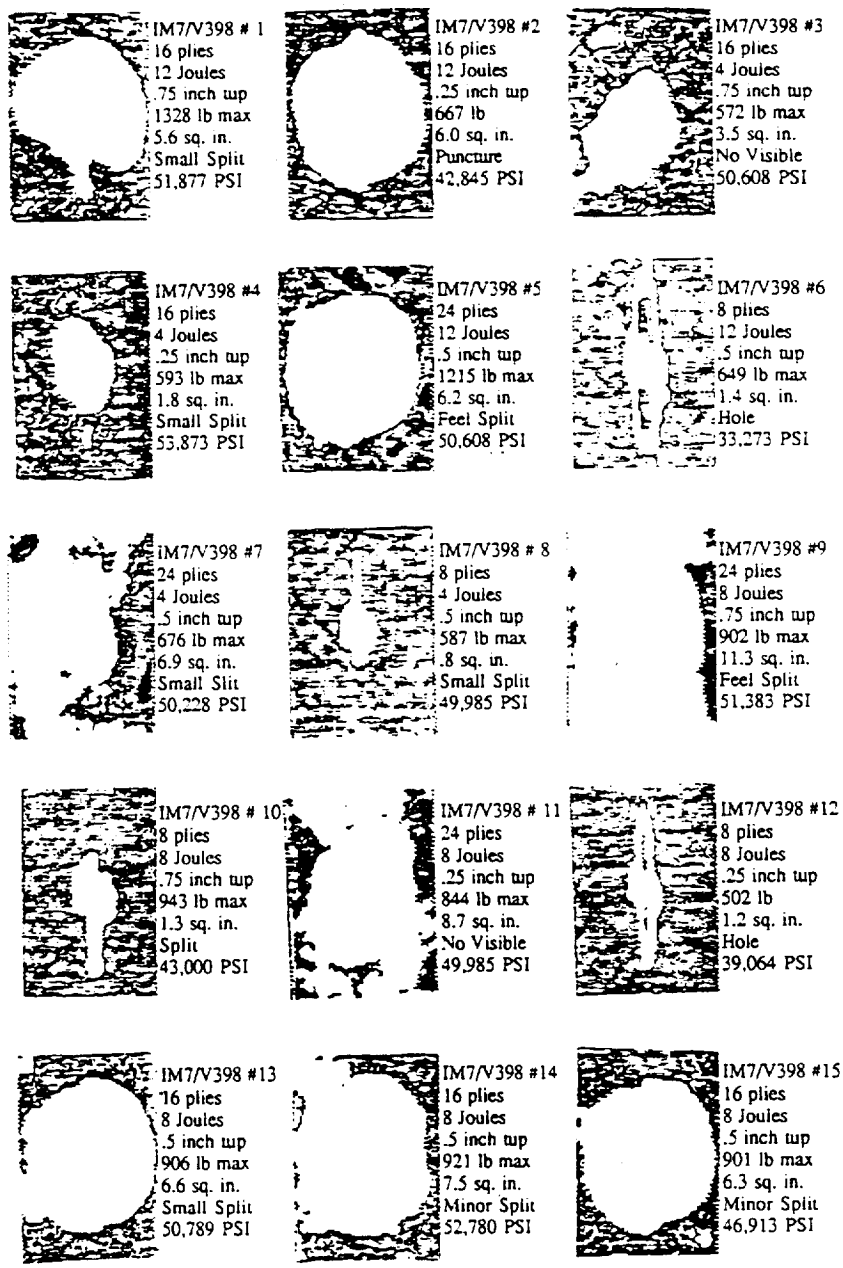

Figure 2c. C-Scans and associated maximum load of impact, damage area, visual damage and residual strength data (IM7/V398).

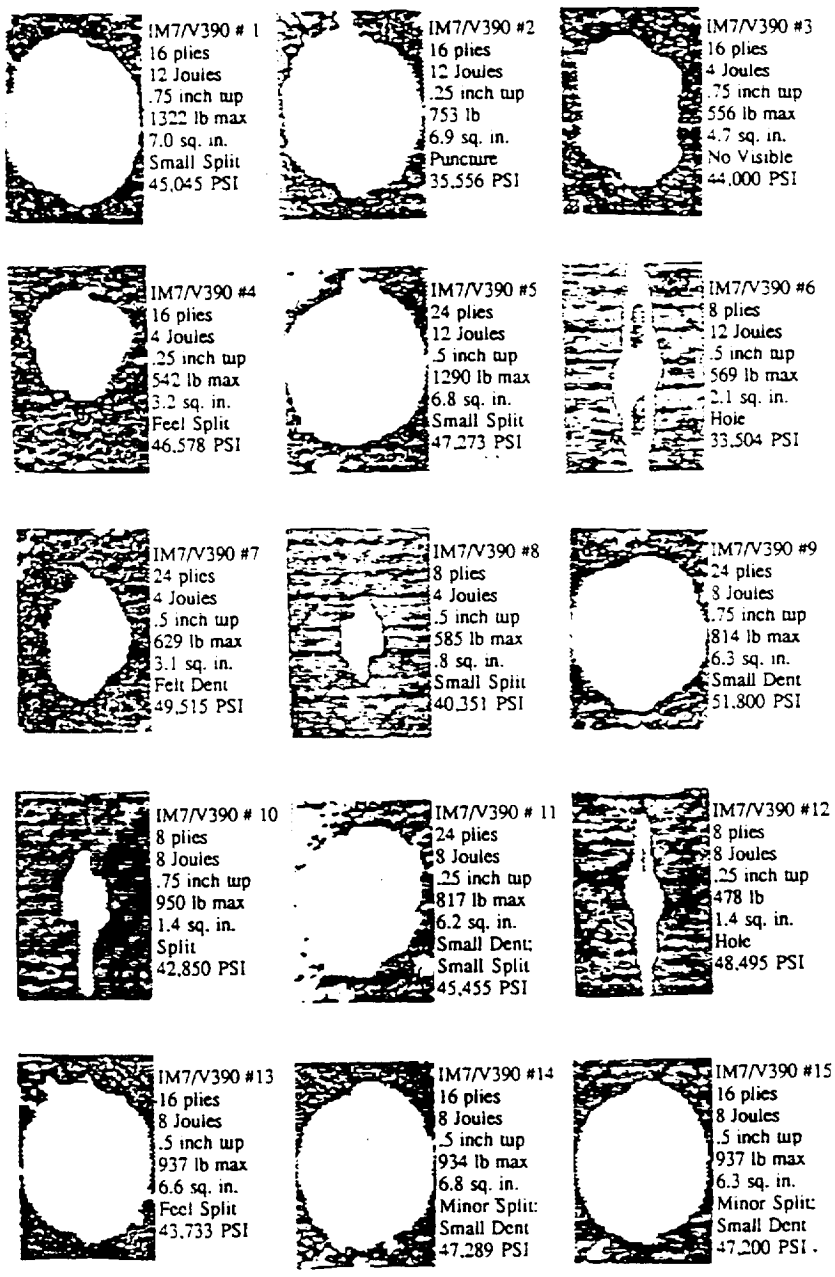

Figure 2d. C-Scans and associated maximum load of impact, damage area, visual damage and residual strength data (IM7/V390).

Material	Interlaminar Shear Stress PSI (90°/-45°) Interface
IM7/977-2	13,167
IM7/F655	12,404
IM7/V390	6,123
IM7/V398	8,820

Figure 3. Short beam shear results.

Response	Constant	Linear Coefficients			Interaction Coefficients			Quadratic Coefficients		
		Energy	Thick	Tup	Energy Thick	Energy Tup	Thick Tup	Energy Energy	Thick Thick	Tup Tup
CAI (MPa)	293	-44	34.5	0	0	0	0	50	0	0
Damage Area (cm^2)	6.6	4.9	-1.4	0	-1.8	0	0	0	1.5	0

Figure 4. Model terms for IM7/977-2 material.

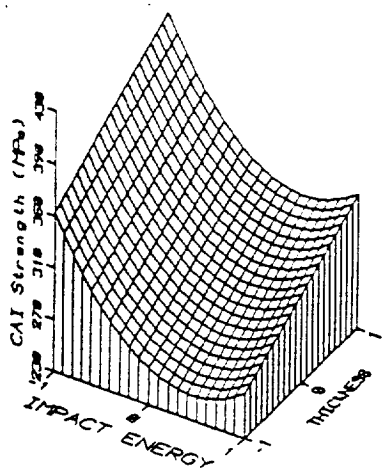

Figure 5. Compression-after-impact strength versus specimen thickness and impact energy for IM7/977-2.

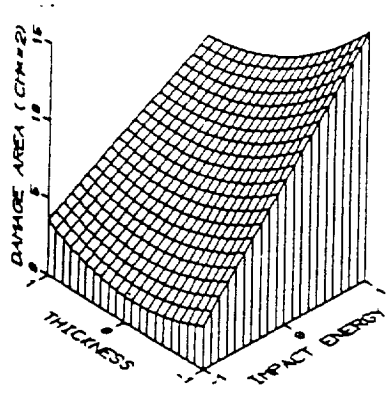

Figure 6. Damage area versus specimen thickness and impact energy for IM7/977-2.

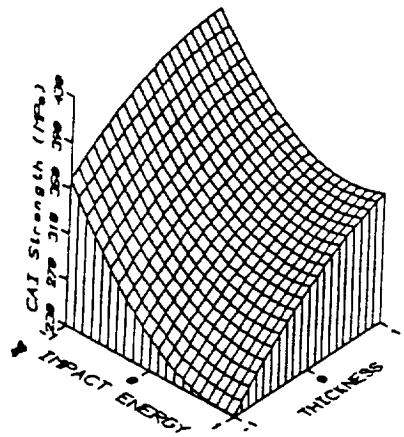

Figure 7. Compression-after-impact strength versus specimen thickness and impact energy for IM7/F655.

Response	Constant	Linear Coefficients			Interaction Coefficients			Quadratic Coefficients		
		Energy	Thick	Tup	Energy Thick	Energy Tup	Thick Tup	Energy Energy	Thick Thick	Tup Tup
CAI (MPa)	318	-53	45	11	11	-7	0	37	-15	0
Damage Area (cm^2)	6.7	5.5	-1.4	2.1	0	3.2	0	1.6	0	1.4

Figure 8. Model terms for IM7/F655 material.

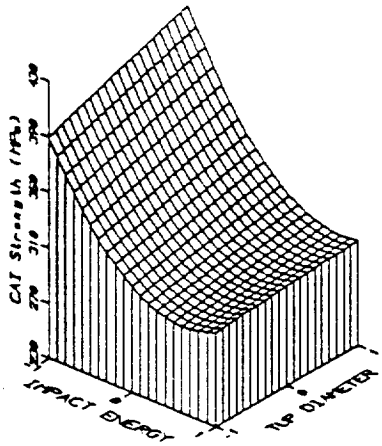

Figure 9. Compression-after-impact strength versus tup size and impact energy for IM7/F655.

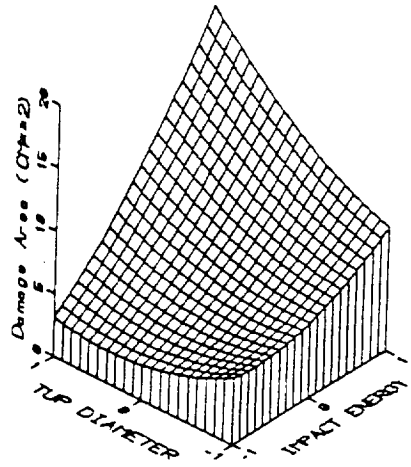

Figure 10. Damage area versus tup size and impact energy for IM7/F655.

Response	Constant	Linear Coefficients			Interaction Coefficients			Quadratic Coefficients		
		Energy	Thick	Tup	Energy Thick	Energy Tup	Thick Tup	Energy Energy	Thick Thick	Tup Tup
CAI (MPa)	352	-14.5	40	9.6	14.5	21	0	-11	-38	0
Damage Area (cm^2)	38	4.9	23	0	0	0	0	-12	0	0

Figure 11. Model terms for IM7/V398 material.

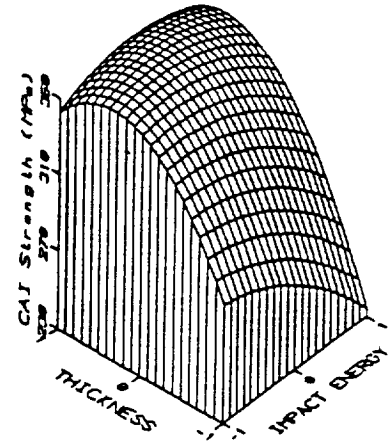

Figure 12. Compression-after-impact strength versus specimen thickness and impact energy for IM7/V398.

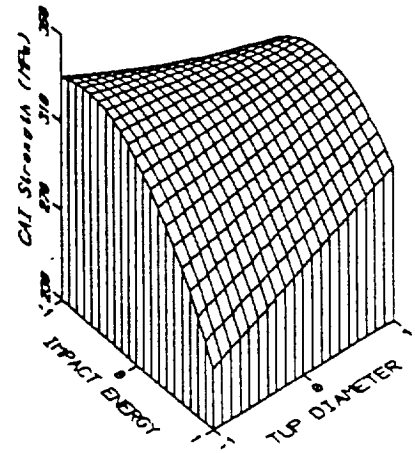

Figure 13. Compression-after-impact strength versus tup size and impact energy for IM7/V398.

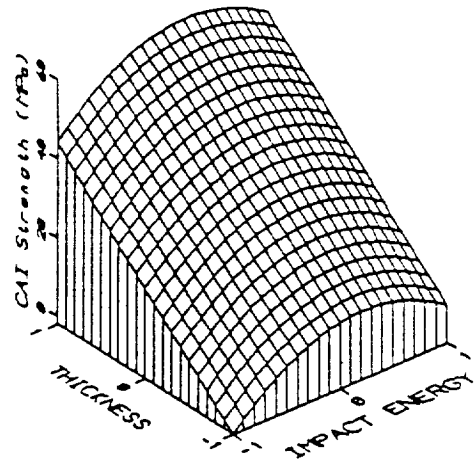

Figure 14. Damage area versus specimen thickness and impact energy for IM7/V398.

Response	Constant	Linear Coefficients			Interaction Coefficients			Quadratic Coefficients		
		Energy	Thick	Tup	Energy Thick	Energy Tup	Thick Tup	Energy Energy	Thick Thick	Tup Tup
CAI (MPa)	323	-16	34.5	0	0	20.5	21	-29	0	0
Damage Area (cm^2)	40.9	9.0	13.5	0	3.8	-2.2	0	-5.1	-15.6	0

Figure 15. Model terms for IM7/V390 material.

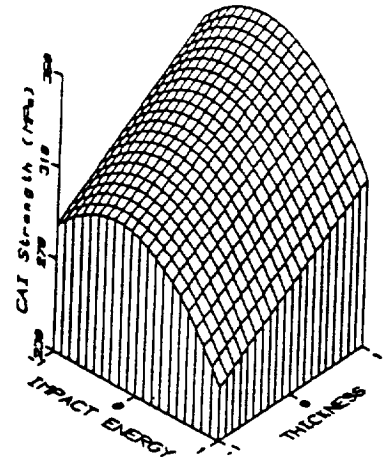

Figure 16. Compression-after-impact strength versus specimen thickness and impact energy for IM7/V390.

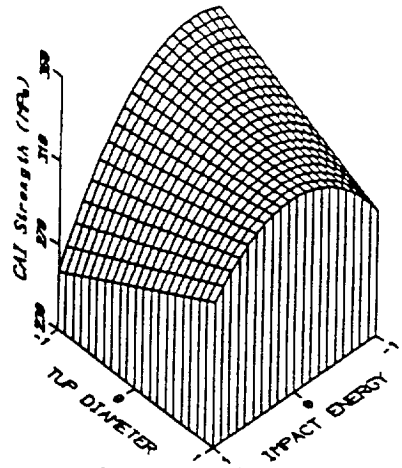

Figure 17. Compression-after-impact strength versus tup size and impact energy for IM7/V390.